IOP Conf. Series: Materials Science and Engineering **735** (2020) 012015 doi:10.1088/1757-899X/735/1/012015

Preparation and Electrochemical Performance of Porous Si/SiOx/G Composite Anode for Lithium Ion Batteries

Jing Wang[1·2·3*], Xiaoyan Zhang[1], Ran Wang[1], Guoqiang Tan[1·2], Yuefeng Su[1·2·3] and Feng Wu[1·2·3]

1. School of Materials Science & Engineering, Beijing Institute of Technology, Beijing Key Laboratory of Environmental Science and Engineering, Beijing, 100081, China.
2. National Development Center of High Technology Green Materials, Beijing, 100081, China.
3. Collaborative Innovation Center of Electric Vehicles, Beijing, 100081, China.
*e-mail: wangjingbit98@bit.edu.cn

Abstract. Silicon/silicon oxides/graphite (Si/SiOx/G) composite with high capacity and excellent cycling performance has been synthesized via high temperature treatment, HF etching and high-energy ball milling for mixture of silicon oxide and graphite. The chemical composition and morphology of the sample was characterized by XRD, SEM and TEM. Large numbers of nanopores were formed in the as-prepared composite, providing three-dimensional transmission pathways for lithium ions and electrons. After 100 cycles, the electrode kept an excellent reversible capacity of 804.2mAh·g^{-1}. The excellent electrochemical properties are mainly attributed to the uniform distribution of silicon particles in amorphous silicon oxide, the buffering effect of porous structure and the improvement of conductivity of the composite by graphite.

1. Introduction

With the development of a series of new technologies such as electric vehicles and portable electronic devices, the lithium-ion batteries (LIBs) with higher energy density have been in widely demand. However, the theoretical capacity of commercial graphite anodes is only 372 mAh·g^{-1}, which hardly continues to be used as the anode material for the next-generation LIBs [1-3]. Therefore, the silicon-based anode with ultra-high theoretical capacity (3580 mAh·g^{-1}) has caused wide attention in recent years and is considered as the most promising anode material for next-generation LIBs. However, the serious volume change (>300%), which will cause destruction and mechanical pulverization of the material structure, severely limits its commercial application. In addition, the electrical conductivity of crystalline silicon is very low and limits its rate performance [4-7].

Compared with crystalline silicon, silicon monoxide (SiO) anode materials have lower volume expansion and better cycle performance, which is favoured by many researchers [8-10]. However, SiO is unstable at high temperature and is prone to dismutase to nano-silicon and silicon oxide (SiOx) or amorphous silicon dioxide, in which the nano-silicon is surrounded by silicon oxide (SiOx). During the first discharge, SiOx can react with lithium to form lithium oxide (Li_2O) and a series of lithium silicate phases, of which lithium silicate phases have a good buffering effect on the volume expansion of silicon. But, the disproportionation of SiO usually happens at high temperature (>900℃) and this process will take a long annealing time. In addition, the prepared nano-silicon is easy to agglomerate to form large particles [11-15]. In this study, NaOH was used to reduce the temperature of

disproportionation of SiO, and a porous silicon-based composite material was prepared by etching with HF, followed by high-energy ball milling with graphite to further reduce the size of particles and improve the electrical conductivity of the composite.

2. Experimental Section

2.1. Material Synthesis

The preparation process of the material is shown in Figure 1. First, 2 g of silicon monoxide powder (SiO, 200 meshes) is mixed with sodium hydroxide solution, and stirred at room temperature. When the solution is evaporated to dryness, it is placed in a tube furnace, heat treated at 700℃ for 30 min in an argon atmosphere. When cooling to room temperature, the prepared material was washed with acetic acid solution to remove sodium silicate formed during the reaction, and the product A was obtained. The product A was added to a 10% HF solution, stirred at room temperature for 10 min, then washed with deionised water until neutral, and dried in an oven at 80℃ to obtain a porous material B (labeled as PSS). The product B and the commercial graphite were put into a planetary ball mill (Fritsch Puluerisette 7, Germany) and the final porous Si/SiOx/Graphite composite (labeled as PSS-G) was obtained.

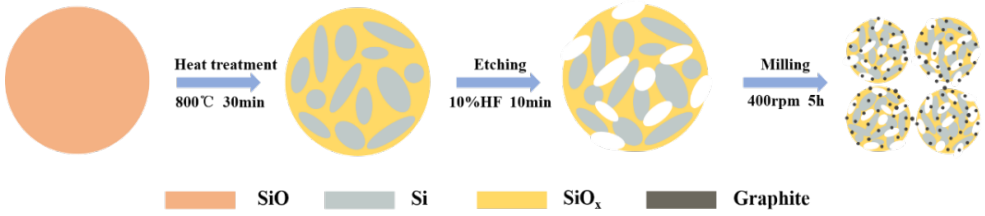

Figure 1. Schematic Illustration of the Synthesis Route of the Si/SiOx/Graphite Composite

2.2. Instruments and Methods

The phase composition of the material was analyzed by X-ray diffractometry (XRD, Ultima IV-185, Japan) with a scanning range of 10° to 80°; the microtopography of the composite was analyzed by scanning electron microscopy (SEM, Hitachi, S-4800) and transmission electron microscopy (TEM); the microstructure of the material was characterized by Raman test (RM, JY Labram HR 800); the surface chemistry of the material was studiedd by X-ray photoelectron spectroscopy (XPS, PHI Quantera).

2.3. Electrochemical Performance

The active material (SiO, PSS, PSS-G), binder (sodium alginate) and acetylene black were mixed at a mass ratio of 70:15:15 to prepare slurry. After casting the slurry on the copper foil, the electrode was dried at 80℃ under vacuum to remove the solvent. Then the film was punched and cut into a circular pole piece with a diameter of 11mm as a working electrode. The coin-type cells were assembled with Li metal as a counter electrode in an Ar-filled glove box, the Celgard 2400 is used as the diaphragm, and the 1 mol/L $LiPF_6$/ (EC+DMC) (volume ratio is 1:1) is used as the electrolyte. Galvanostatic charge/discharge were carried out on a battery testing system(Land CT2100A) within a voltage window of 0.01-2.0 V with current density of 100mA·g^{-1}. Cyclic voltammetry (CV) measurement and impendance testing were performed on a electrochemical workstation (CHI 660E).

3. Results and Discussion

3.1. Structure and Morphology

Figure 2a shows XRD patterns of original SiO, porous material PSS (product B) and PSS-G composite. In the XRD pattern of the original SiO, a diffuse peak appeared between 20° and 30°, indicating that SiO is amorphous. Two sharp peaks appeared at 26.6° and 28.4° respectively, indicating that crystalline SiO_2 and Si phases are present in the original SiO. The XRD pattern of PSS sample shows

obvious diffraction peaks of crystalline Si (PDF#27-1402) and cristobalite (PDF#39-1425), which indicates that the disproportionation reaction of SiO occurs after heat treatment at 700 ℃. The reaction process is $3SiO + 2NaOH = Na_2SiO_3 + H_2\uparrow + Si + SiO_2$, and the amorphous SiO_2 is converted into a crystalline state of cristobalite in the presence of NaOH [16]. According to the *Scherrer* formula, the average particle sizes of the cristobalite and crystalline Si are 20 nm and 14 nm, respectively [17]. In the XRD pattern of PSS-G, the peaks of graphite appeared at 26.5°, 44.5° and 54.7°, and the diffraction peaks of crystalline Si and cristobalite are still existed, indicating that the ball milling did not destroy the crystal structure of the material. Figure 2b is the Raman spectrum of PSS-G composites, the peaks of D-band and G-band appeared around 1360 cm^{-1} and 1580 cm^{-1} due to the addition of graphite. The weak peak appearing around 520 cm^{-1} proves the presence of crystalline silicon in the PSS-G, which consistents with the XRD results. Figure 2c shows the XPS (Si 2p) spectrum of the PSS-G composite, which contains silicon species in the valence state of Si^{4+}, Si^{3+}, Si^{2+}, Si^{1+} and Si^0, and with the highest content of Si^{3+}, indicating that the silicon in the composite is mainly in the form of silicon oxide, and the appearance of Si^0 also indicates that the crystalline silicon is generated during the disproportionation.

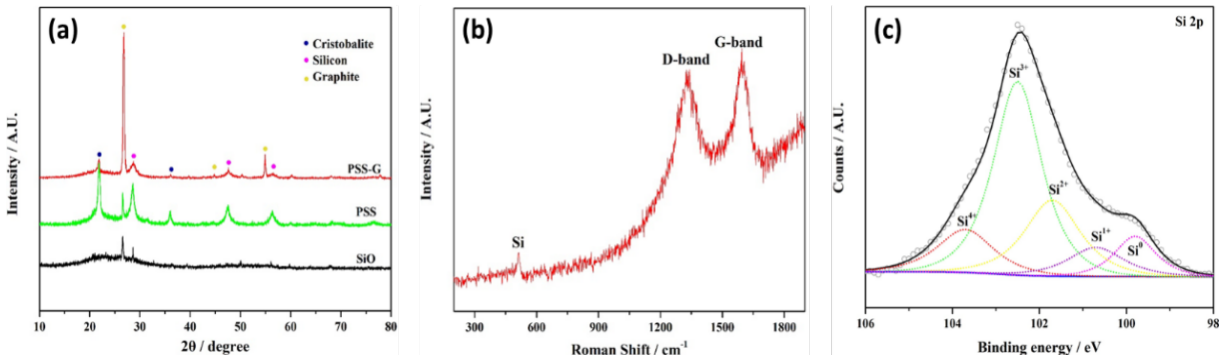

Figure 2. (a) XRD Patterns of Sample SiO, PSS and PSS-G, (b) Roman and (c) XPS Si 2p Spectra of PSS-G Composite

Figure 3 is the morphology images of graphite, SiO and PSS (product B). Figure 3a shows that graphite has a sheet-like structure with a particle size on the level of micronanometers. In Figure 3b, the morphology of SiO is irregular, the surface of the particles is smooth and has sharp edges and corners, and the particle size is about 20-40μm. Figure 3d shows that after high temperature heat treatment and HF etching, the surface of the material particles becomes rough, and many pores appear on the surface to form a porous structure, which can provide a three-dimensional channel for the transport of lithium ions. The material in Figure 3e is flocculated, indicating that a porous structure appears in the material after HF etching. A large number of nanocrystalline particles appear in Figure 3f and are surrounded by amorphous silicon oxide, which illustrating the formation of a crystalline Si and cristobalite phase in the disproportionation reaction, this corresponds to the XRD pattern.

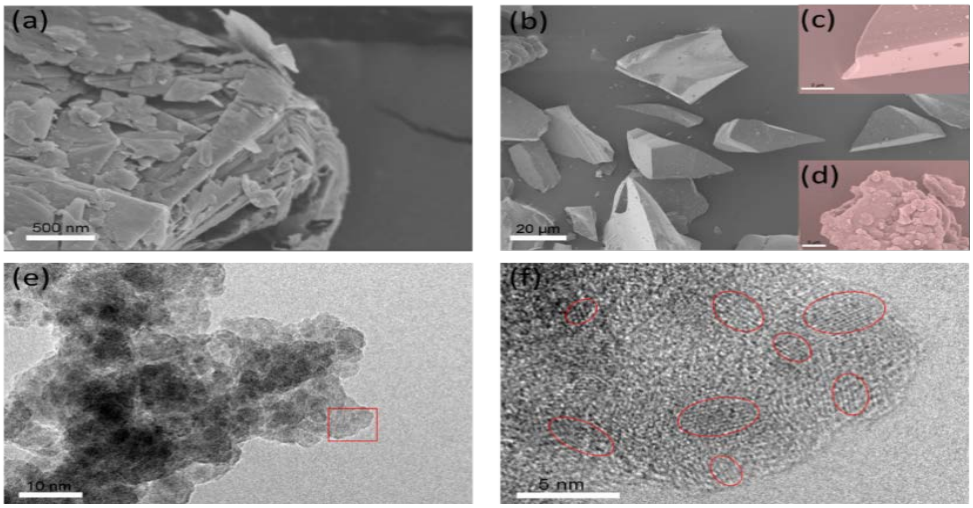

Figure 3. SEM Images of Sample (a) Graphite, (b and c) SiO, (d) PSS and TEM Images of (e and f) PSS Composite

3.2. Electrochemical Properties

Figure 4a is the CV curve of PSS-G composite electrode. In the first lithium intercalation process, there is a broad reduction peak between 0.6-1.0V, corresponding to the decomposition of electrolyte to form the SEI film [18], but the reduction peak disappeared from the second cycle and the curve becomes smoother. There is a sharp reduction peak near 0 V, which corresponds to the intercalation of lithium into bulk silicon. The anode peaks at 0.33V and 0.52V correspond to the delithiation process of SiO [19], and its intensity is continuously enhanced during the subsequent cycles, but the peak position does not move significantly, which indicates that the kinetic enhancement process occurs on the electrode.

Figure 4b shows the charge-discharge curve for the first three cycles of PSS-G electrode. The ICE of the PSS-G electrode is 62.2%, which has a large increase compared to pure SiO (49.8%). But the PSS-G electrode still has a large capacity loss, mainly because the irreversible reaction of SiO during the first cycle, which consumes a large amount of Li^+ to form electrochemically inert Li_2O, Li_3SiO_3, Li_4SiO_4 and so on. The Coulombic efficiency increased rapidly during the next series cycles, which indicating that the SEI film tends to be stable.

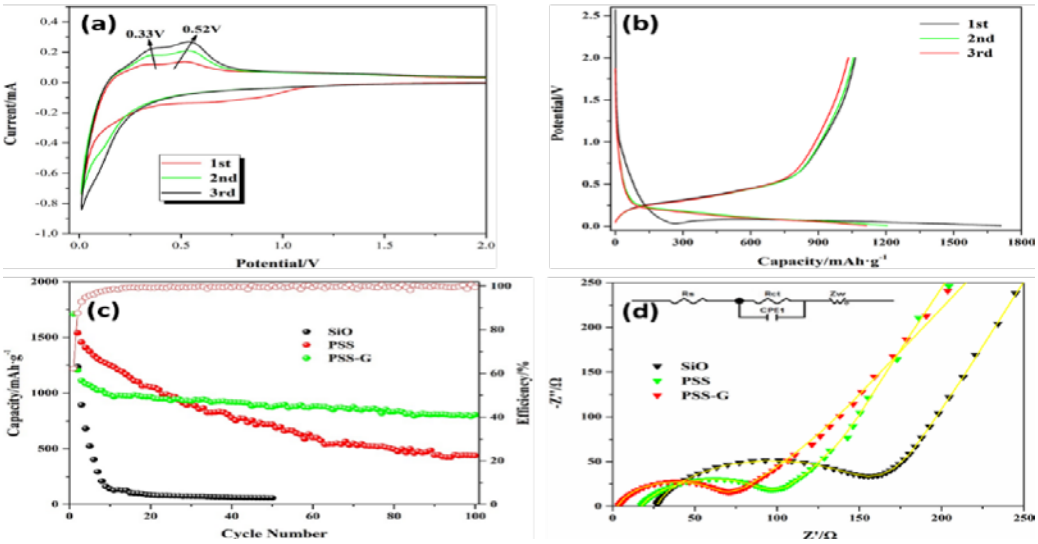

Figure 4. (a) CV and (b) the Charge-discharge Curves of PSS-G Composite Electrode, (c) Cycle Performance and (d) Nyquist Plots of Sample SiO, PSS and PSS-G

Figure 4c shows the cycle performance of sample SiO, PSS and PSS-G. Although the capacity of pure SiO can reach to 2305.5 $mAh \cdot g^{-1}$ in the first cycle, the reversible capacity decreased rapidly as the cycle proceeded. After 17 cycles, the capacity was lower than 100 $mAh \cdot g^{-1}$. After high temperature treatment and HF etching, the first cycle capacity of the PSS electrode increased to 2535.5 $mAh \cdot g^{-1}$, and the cycle stability was also improved. This is mainly because the nano-Si particles generated during the disproportionation process are surrounded by the amorphous silicon oxide, which can alleviate the volume effect of nano-Si. Also, partial silicon oxide was etched by HF to form large number of pores, which can reduce the stress change during cycling and can also buffer the volume expansion. However, the capacity of PSS electrode decreased in the subsequent cycles, this is mainly because of the low electrical conductivity of Si and destruction of material structure in cycling. When the PSS and graphite are mixed by ball milling, the cycle stability of the material is further improved. The reason for this is that, on the one hand, the particle size decreases after ball milling, and the stress variation due to volume change during cycling is reduced; On the other hand, graphite has a good conductivity, it can ensure good electrical contact between particles, reducing the possibility of peeling off between active silicon particles for particles. Therefore, the PSS-G composite exhibits a good electrochemical cycle stability, and its reversible capacity can reach 804.2 $mAh \cdot g^{-1}$ after 100 cycles.

Figure 4d shows the Nyquist plots of sample SiO, PSS and PSS-G. Each of the curves has a similar shape which consists of a semicircle and a straight sloping line. The semicirclele indicates the charge-transfer resistance (Rct) and the sloping line indicates the diffusion impedance (Zw) of Li^+ in materials. Obviously, the three curves have significant differences in the electrochemical impedance parameters [20]. Table1 shows the electrochemical impedance parameters of the three electrodes. It can be seen from Table 1 that the PSS-G electrode has the lowest charge transfer impedance, indicating that ball milling and the addition of graphite improves the rate of charge transfer between the interfaces. In addition, there also has a large difference between the ohmic impedances. The data in Table 1 shows that the PSS-G electrode has the lowest ohmic resistance value of 4.0Ω, which indicates that the addition of graphite also improves the electrical contact between the electrode material and the current collector, the structural pulverization of the material and the isolation of the active particles caused by the volume expansion of the material during cycling are avoided, so the cycle stability is improved.

Table 1. Electrochemical Impedance Parameters of the Three Electrodes

Sample	Rs(Ω)	Rct(Ω)
SiO	27.2	102.3
PSS	17.8	78.6
PSS-G	4.0	63.2

4. Conclusion

Porous Si/SiOx/Graphite composite anode materials were prepared by commercial SiO and graphite by high temperature heat treatment, HF etching and high energy ball milling. The nano-Si particles generated by the disproportionate reaction in the composite material are uniformly coated by the silicon oxide substrate. In addition, the material is etched by HF to form a porous structure, which can buffer the volume expansion of silicon, so the cycle performance of SiO was obviously improved. The high-energy ball milling further reduces the size of the particles, the electrical conductivity and cycle performance of the material are further improved with the addition of graphite which acts as a "connection medium" between the active material particles and the current collectors. At a current density of 100$mA \cdot g^{-1}$, the reversible capacity was 804.2 $mAh \cdot g^{-1}$ after 100 cycles, and no obvious capacity decline was found.

5. Acknowledgments
This work was financially supported by the National Key R&D Program of China(2018YFB0104401).

6. References

[1] J.M. Tarascon, M. Armand, Issues and challenges facing rechargeable lithium batteries, *NATURE*, 414(6861), 359(2001)
[2] M. Armand, J.M. Tarascon, Building better batteries, *NATURE*, 451(7179), 652(2008)
[3] H. Li, Z.X. Wang, L.Q. Chen, X.J. Huang, Research on Advanced Materials for Li-ion Batteries, *Advanced materials*, 21(45), 4593(2009)
[4] C.K. Chan, H.L. Peng, G. Liu, K. Mcilwrath, X.F. Zhang, R.A. Huggins, Y. Cui, High-performance lithium battery anodes using silicon nanowires, *Nature nanotechnology*, 3(1), 31(2008)
[5] Y.S. Hu, R. Demir-Cakan, M.M. Titirici, J.O. Muller, R. Schlogl, M. Antonietti, J. Maier, Superior storage performance of a Si@SiOx/C nanocomposite as anode material for lithium-ion batteries, *Angew. Chem. Int. Ed.*, 47(9), 1645(2008)
[6] H. Gao, L.S. Xiao, I. Plumel, G.L. Xu, Y. Ren, X.B. Zuo, Y.Z. Liu, C. Schulz, H. Wiggers, K. Amine, Z.H. Chen, Parasitic Reactions in Nanosized Silicon Anodes for Lithium-Ion Batteries, *Nano Lett.*, 17(3), 1512(2017)
[7] J. Ryu, D. Hong, M. Shin, S. Park, Multiscale Hyperporous Silicon Flake Anodes for High Initial Coulombic Efficiency and Cycle Stability, *ACS nano*, 10(11), 10589(2016)
[8] C.H. Doh, C.W. Park, H.M. Shin, D.H. Kim, Y.D. Chung, S.I. Moon, B.S. Jin, H.S. Kim, A. Veluchamy, A new SiO/C anode composition for lithium-ion battery, *Journal of Power Sources*, 179(1), 367(2008)
[9] J.H. Yom, S.W. Hwang, S.M. Cho, W.Y. Yoon, Improvement of irreversible behavior of SiO anodes for lithium ion batteries by a solid state reaction at high temperature, *Journal of Power Sources*, 311, 159(2016)
[10] J. Woo, S.H. Baek, A comparative investigation of different chemical treatments on SiO anode materials for lithium-ion batteries: towards long-term stability, *RSC Adv.*, 7(8), 4501(2017)
[11] C.M. Park, W. Choi, Y. Hwa, J.H. Kim, G. Jeong, H.J. Sohn, Characterizations and electrochemical behaviors of disproportionated SiO and its composite for rechargeable Li-ion batteries, *Journal of Materials Chemistry*, 20(23), 4854(2010)
[12] Y.R. Ren, M.Q. Li, Si-SiOx-Cristobalite/Graphite Composite as Anode for Li-ion Batteries, *Electrochimica Acta*, 142, 11(2014)
[13] S.Z. Zeng, X.R. Zeng, L. Huang, H.L. Wu, Y.C. Yao, X.F. Zheng, J.Z. Zou, The formation mechanisms of porous silicon prepared from dense silicon monoxide, *RSC Adv.*, 7(13), 7990(2017)
[14] B.C. Yu, Y. Hwa, C.M. Park, H.J. Sohn, Reaction mechanism and enhancement of cyclability of SiO anodes by surface etching with NaOH for Li-ion batteries, *Journal of Materials Chemistry A*, 1(15), 4820(2013)
[15] J.I. Lee, K.T. Lee, J. Cho, J. Kim, N.S. Choi, S. Park, Chemical-assisted thermal disproportionation of porous silicon monoxide into silicon-based multicomponent systems, *Angewandte Chemie*, 51(11), 2767(2012)
[16] J.I. Lee, N.S. Choi, S. Park, Highly stable Si-based multicomponent anodes for practical use in lithium-ion batteries, *Energy & Environmental Science*, 5(7), 7878(2012)
[17] B.D. Cullity, Elements of X-Ray Diffraction, *Addison-Wesley*, (1978)
[18] H. Tang, J.P. Tu, X.Y. Liu, Y.J. Zhang, S. Huang, W.Z. Li, X.L. Wang, C.D. Gu, Self-assembly of Si/honeycomb reduced graphene oxide composite film as a binder-free and flexible anode for Li-ion batteries, *Journal of Materials Chemistry A*, 2(16), 5834(2014)
[19] J. Wang, M. Zhou, G. Tan, S. Chen, F. Wu, J. Lu, K. Amine, Encapsulating micro-nano Si/SiOx into conjugated nitrogen-doped carbon as binder-free monolithic anodes for advanced lithium ion batteries, *Nanoscale*, 7(17), 8023(2015)

[20] X. Yu, H. Yang, H. Meng, Y. Sun, J. Zheng, D. Ma, X. Xu, Three-Dimensional Conductive Gel Network as an Effective Binder for High-Performance Si Electrodes in Lithium-Ion Batteries, *ACS applied materials & interfaces*, 7(29), 15961(2015)